

Geometrically thick tori around compact objects with a quadrupole moment

Jan-Menno Memmen and Volker Perlick

ZARM, University of Bremen, 28359 Bremen, Germany.

Email: jan.memmen@zarm.uni-bremen.de, volker.perlick@zarm.uni-bremen.de

Abstract. We study geometrically thick perfect-fluid tori with constant specific angular momentum, so-called “Polish doughnuts”, orbiting deformed compact objects with a quadrupole moment. More specifically, we consider two different asymptotically flat, static and axisymmetric vacuum solutions to Einstein’s field equation with a non-zero quadrupole moment, the q -metric and the Erez-Rosen spacetime. It is our main goal to find features of Polish doughnuts in these two spacetimes which qualitatively distinguish them from Polish doughnuts in the Schwarzschild spacetime. As a main result we find that, for both metrics, there is a range of positive (Geroch-Hansen) quadrupole moments which allows for the existence of double tori. If these double tori fill their Roche lobes completely, their meridional cross-section has the shape of a fish, with the body of the fish corresponding to the outer torus and the fish-tail corresponding to the inner torus. Such double tori do not exist in the Schwarzschild spacetime.

1. Introduction

As no signal can escape from a black hole, detecting a black hole is a non-trivial task. Recently, gravitational waves from merging black holes have been observed [1]. However, these events are still comparatively rare, and they require two black holes spiralling onto each other. Static or stationary black holes cannot be detected this way, as they do not emit any gravitational waves. Hence, the only way of observing such a black hole is via its influence on matter or light rays in its vicinity.

For studying the gravitational influence on matter one may consider a black hole that is surrounded by a geometrically thick perfect-fluid torus. An analytical treatment is possible if one assumes that (i) the matter can be approximated as stationarily rotating (over a comparatively long time), without actually approaching the black hole, and (ii) the self-gravity of the fluid body can be neglected. For the simplest cases of a Schwarzschild and a Kerr black hole, such stationarily rotating perfect-fluid tori have been found, in the form of exact analytical solutions to the relativistic Euler equation, by a group of Polish scientists (see Jaroszyński et al. [2] for the original article, and also Rezzolla and Zanotti [3] for a review), and they are now known as *Polish doughnuts*.

Such tori exist not only around black holes, but also around any other object that is sufficiently compact. As such objects could be easily mistaken for black holes, they

are known as *black hole impostors* or *black hole mimickers*. Recall that according to the black-hole uniqueness theorem a black hole is spherically symmetric if it is non-rotating and isolated. More specifically, this theorem implies that, if the spacetime around a black hole is a static and asymptotically flat solution to Einstein's vacuum field equation, then it is the Schwarzschild solution, i.e., all of its (Geroch-Hansen) multipole moments vanish with the exception of the monopole term. By contrast, the asymptotically flat and static vacuum spacetime around a black-hole impostor may have arbitrary mass multipole moments. In particular, it may have a non-zero quadrupole moment which, for a non-rotating and axisymmetric object, could be considered as the leading-order deviation from the Schwarzschild metric. This raises the question of whether such a non-zero quadrupole moment has a characteristic influence on the shape of Polish doughnuts, which would allow to distinguish such impostors from black holes. This is the question we want to investigate in this paper.

To that end, we construct Polish doughnuts in two spacetimes which describe the exterior of a source with a non-zero quadrupole moment. Both spacetimes are static, axisymmetric and asymptotically flat solutions to Einstein's vacuum field equation, i.e., they describe the vacuum region around a non-rotating and isolated central object. The first one is the so-called q -metric, which, in the form considered here, was found by Quevedo [4]; the second one is the Erez-Rosen metric [5]. These metrics do not feature a horizon, i.e., they do not describe the spacetime around a black hole, unless in the case of a vanishing quadrupole moment where they reduce to the Schwarzschild metric. If extended to sufficiently low radii, they rather display a naked singularity. As many physicists consider such naked singularities as unphysical, one may replace the metric in an inner region of the spacetime by an interior (e.g. perfect-fluid) solution to Einstein's field equation, and then match it to the exterior vacuum spacetime at a surface arbitrarily close to the naked singularity. In this way, both the q -metric and the Erez-Rosen metric can be interpreted as viable models for the spacetime around an object with a quadrupole moment that may be very compact but not compact enough for having collapsed to a black hole. With this interpretation, these two metrics make very good black-hole impostors.

The paper is organised as follows. In section 2, we review relevant background material for constructing Polish doughnuts in an arbitrary axisymmetric and static spacetime. In section 3, we specify this to the q -metric, and in section 4, we specify it to the Erez-Rosen metric. It is our main goal to find out whether or not the accretion tori in these two spacetimes have common features that distinguish them from accretion tori around a non-rotating and isolated black hole, i.e., from accretion tori in the Schwarzschild metric.

We use geometrised units ($c = G = 1$) and our convention for the metric signature is $(-, +, +, +)$. Greek indices are running from 0 to 3 and Einstein's summation convention is applied. As usual, we raise and lower indices with the spacetime metric.

2. Circular motion in static axisymmetric spacetimes

We consider a static axisymmetric metric,

$$g_{\mu\nu}dx^\mu dx^\nu = g_{tt}dt^2 + g_{rr}dr^2 + g_{\vartheta\vartheta}d\vartheta^2 + g_{\varphi\varphi}d\varphi^2, \quad (1)$$

where the metric coefficients $g_{\mu\nu}$ are independent of t and φ . We denote the corresponding Killing vector fields by

$$\eta^\mu = \delta_t^\mu, \quad \xi^\mu = \delta_\varphi^\mu. \quad (2)$$

We restrict to the part of the spacetime where $g_{\varphi\varphi} > 0$ and $g_{tt} < 0$.

In this preparatory section, we want to summarise some properties of matter particles that are in circular (in general non-geodesic) uniform motion about the symmetry axis of the spacetime. Then the four-velocity $u^\mu \partial_\mu$ has to satisfy $u^r = u^\vartheta = 0$ and can be written as

$$u^\mu = u^t(\eta^\mu + \Omega\xi^\mu),$$

where

$$\Omega = \frac{u^\varphi}{u^t} = \frac{d\varphi}{dt} \quad (3)$$

is the coordinate angular velocity. By uniformity, Ω depends only on r and ϑ . From the normalisation condition $g_{\mu\nu}u^\mu u^\nu = -1$, we find

$$(u^t)^{-2} = -g_{tt} - \Omega^2 g_{\varphi\varphi}. \quad (4)$$

As $(u^t)^{-2}$ must be positive, this equation restricts Ω as a function of r and ϑ .

We may also characterise the motion by the *specific angular momentum*

$$l = -\frac{u_\varphi}{u_t} = -\frac{g_{\varphi\varphi}u^\varphi}{g_{tt}u^t}. \quad (5)$$

It is related to the angular velocity Ω by the equation

$$g_{\varphi\varphi}\Omega = -g_{tt}l, \quad (6)$$

so we can prescribe the motion either by specifying Ω as a function of r and ϑ , or equivalently by specifying l as a function of r and ϑ . If rewritten in terms of l , Eq. (4) reads

$$u_t^{-2} = -g^{tt} - l^2 g^{\varphi\varphi}. \quad (7)$$

As u_t^{-2} is positive, this equation restricts the values of l that are allowed at a certain point (r, ϑ) .

For the visualisation of circular motion in an axisymmetric and static spacetime, one often uses the so-called *von Zeipel cylinders*, which are defined as the surfaces of constant *von Zeipel radius* \mathcal{R} ,

$$\mathcal{R}^2 = \frac{l}{\Omega} = -\frac{g_{\varphi\varphi}}{g_{tt}}. \quad (8)$$

In flat spacetime, where $g_{tt} = -1$ and $g_{\varphi\varphi} = r^2 \sin^2 \vartheta$, they reduce to the ordinary Euclidean cylinders, $\mathcal{R}^2 = r^2 \sin^2 \vartheta$. The relativistic notion of von Zeipel cylinders was

introduced by Abramowicz [6], who showed that these cylinders are always perpendicular to the direction of the centrifugal acceleration. Remarkably, they are the same for *all* circular motions, independent of the angular velocity. The fact that the left-hand side of Eq. (7) must be positive can now be written as

$$l^2 < \mathcal{R}^2, \quad (9)$$

i.e., the region where circular motion is possible with a certain specific angular momentum l is bounded by the von Zeipel cylinder $\mathcal{R}^2 = l^2$.

2.1. Effective potential and geometrically thick tori

We now recall some basic facts about perfect fluids in circular motion on an axisymmetric static spacetime. For details and derivations, we refer to Rezzolla and Zanotti [3]. Using the angular velocity Ω and the specific angular momentum l introduced above, the Euler equation for a perfect fluid in the case of circular motion reduces to

$$\partial_\mu \ln |u_t| - \left(\frac{\Omega}{1 - \Omega l} \right) \partial_\mu l = -\frac{1}{\rho h} \partial_\mu p \quad (10)$$

where ρ is the energy density, p is the pressure and h is the specific enthalpy.

Here we assume that the fluid shares the symmetry of the spacetime, which implies that u_t , Ω , l , ρ , p and thus h are functions of r and ϑ only. For a barotropic fluid, ρ , and thus h , are functions of p , so the right-hand side of (10) becomes a differential. By differentiating both sides, it becomes apparent that the differentials dl and $d\Omega$ are linearly dependent. This implies that either $dl = 0$ or $\Omega = \Omega(l)$. This result is known as the (relativistic) *von Zeipel theorem*.

If dl has no zeros, the Euler equation (10) can be integrated to [6]

$$\mathcal{W} - \mathcal{W}_{\text{in}} := - \int_0^p \frac{dp'}{\rho h} = \ln |u_t| - \ln |(u_t)_{\text{in}}| - \int_{l_{\text{in}}}^l \frac{\Omega}{1 - \Omega l'} dl' \quad (11)$$

where the last integral makes sense because Ω is a function of the specific angular momentum. Here \mathcal{W} is an *effective potential* which is defined only up to an arbitrary constant, and the suffix “in” stands for the value of the corresponding quantity at some chosen point; for the construction of perfect-fluid tori one usually chooses this point at the inner edge of the torus.

If, on the other hand, dl is identically zero, i.e, if we consider a barotropic fluid with constant specific angular momentum, then Eq. (11) is also true, but now the last integral in this equation vanishes. With the help of Eq. (7), we then find that the effective potential can be expressed as

$$\mathcal{W}(l, r, \vartheta) = -\frac{1}{2} \ln \left(-g^{tt}(r, \vartheta) - l^2 g^{\varphi\varphi}(r, \vartheta) \right) \quad (12)$$

where we have chosen the arbitrary additive constant in \mathcal{W} such that $\mathcal{W}_{\text{in}} = \ln |(u_t)_{\text{in}}|$. Equation (12) determines circular motion of a perfect fluid with constant specific angular momentum l . Stationarily rotating perfect-fluid tori with this property are known as “Polish doughnuts”. They have been discussed first by Jaroszyński, Abramowicz and

Paczyński in Schwarzschild and Kerr spacetimes [2]; for a detailed review of the topic, we refer again to Rezzolla and Zanotti [3].

The relation between the potential \mathcal{W} , the density ρ and the pressure p can be calculated explicitly if we assume a polytropic equation of state

$$p(r, \vartheta) = K \rho(r, \vartheta)^\Gamma, \quad h(r, \vartheta) = 1 + \frac{K \Gamma \rho(r, \vartheta)^{\Gamma-1}}{\Gamma - 1} \quad (13)$$

where $\Gamma > 1$ and $K > 0$ are constants, known as the polytropic index and the polytropic constant, respectively. Then we can evaluate the integral after the first equality sign in Eq. (11). This gives ρ , and thereby p , explicitly in terms of the effective potential \mathcal{W} ,

$$\rho(r, \vartheta) = \left[\left(\frac{\Gamma - 1}{K\Gamma} \right) \left(e^{\mathcal{W}_{\text{in}} - \mathcal{W}(l, r, \vartheta)} - 1 \right) \right]^{\frac{1}{\Gamma-1}}. \quad (14)$$

Note that there are two parameters, l and \mathcal{W}_{in} , which we can choose freely. As the density ρ must be non-negative, the fluid body is restricted to the region where $\mathcal{W}(l, r, \vartheta) \leq \mathcal{W}_{\text{in}}$. The equation $\mathcal{W}(l, r, \vartheta) = \mathcal{W}_{\text{in}}$ determines the boundary of the fluid body. By fixing l , we specify the potential surfaces $\mathcal{W} = \text{constant}$, and by fixing the value of \mathcal{W}_{in} , we single out a particular equipotential surface as the boundary of the fluid body. Note that the parameters that enter into the equation of state have no influence on the shape of the fluid body. They do, however, influence the distribution of density and pressure in the fluid.

We are interested in the case that l and \mathcal{W}_{in} have been chosen such that the equation $\mathcal{W}(l, r, \vartheta) = \mathcal{W}_{\text{in}}$ describes a simple closed curve in the r - ϑ -plane, which means that the fluid occupies the interior of a torus. This is the situation the name “Polish doughnut” refers to. In this situation, the potential $\mathcal{W}(l, r, \vartheta)$, the density $\rho(r, \vartheta)$ and the pressure $p(r, \vartheta)$ must have a critical point at some $(r_{\text{cen}}, \vartheta_{\text{cen}})$ inside the fluid, called the “centre” of the doughnut. If we restrict to the case that the density, and consequently the pressure, varies monotonically between the centre and the boundary, this critical point must be a local maximum for ρ and p , i.e., a local minimum for \mathcal{W} . In the spacetimes considered below, we will have

$$\left. \frac{\partial \mathcal{W}(l, r, \vartheta)}{\partial \vartheta} \right|_{\vartheta=\pi/2} = 0, \quad \left. \frac{\partial^2 \mathcal{W}(l, r, \vartheta)}{\partial \vartheta^2} \right|_{\vartheta=\pi/2} > 0. \quad (15)$$

Then a critical point of the potential in the equatorial plane is characterised by the equation

$$\left[\frac{\partial g^{tt}(r, \vartheta)}{\partial r} + l^2 \frac{\partial g^{\varphi\varphi}(r, \vartheta)}{\partial r} \right]_{\vartheta=\pi/2} = 0. \quad (16)$$

This critical point is a minimum of the potential if

$$\pm \left[\frac{\partial^2 g^{tt}(r, \vartheta)}{\partial r^2} + l^2 \frac{\partial^2 g^{\varphi\varphi}(r, \vartheta)}{\partial r^2} \right]_{\vartheta=\pi/2} > 0 \quad (17)$$

holds with the upper sign, and it is a saddle if this inequality holds with the lower sign. So, for the construction of Polish doughnuts, we will have to choose l such that there is a point $(r_{\text{cen}}, \vartheta_{\text{cen}} = \pi/2)$ where (16) and (17) with the upper sign hold.

The fact that the differential of p vanishes at the centre implies that a fluid element at $(r_{\text{cen}}, \vartheta_{\text{cen}})$ moves along a circular timelike geodesic. This follows immediately from the fact that, quite generally, the Euler equation reduces to the geodesic equation at points where dp vanishes. For this reason, circular geodesics play an important role in the construction of Polish doughnuts, so we will now briefly discuss some of their properties.

2.2. Circular geodesics

As before we consider a static and axisymmetric spacetime, see Eq. (1), but now we assume in addition that the spacetime is symmetric with respect to the equatorial plane $\vartheta = \pi/2$. Then a geodesic starting tangentially to this plane will remain in this plane. In this section we want to calculate the circular timelike and lightlike geodesics in the equatorial plane; their properties will become important later. To that end we recall that geodesics in the equatorial plane derive from the Lagrangian

$$\mathcal{L} = \frac{1}{2} \left(g_{tt} \dot{t}^2 + g_{rr} \dot{r}^2 + g_{\varphi\varphi} \dot{\varphi}^2 \right) \quad (18)$$

where the metric coefficients depend on r only, as $\vartheta = \pi/2$. In the following we write $g_{\mu\nu}(r)$ instead of $g_{\mu\nu}(r, \vartheta = \pi/2)$ for the sake of brevity.

There are three constants of motion

$$E = -g_{tt}(r)\dot{t}, \quad L = g_{\varphi\varphi}(r)\dot{\varphi}, \quad \varepsilon = -g_{tt}(r)\dot{t}^2 - g_{rr}(r)\dot{r}^2 - g_{\varphi\varphi}(r)\dot{\varphi}^2 \quad (19)$$

where $\varepsilon = 0$ for lightlike and $\varepsilon = 1$ for timelike geodesics. The first two equations imply

$$l = \frac{L}{E} \quad (20)$$

where l is the specific angular momentum defined in (5). Combining the three equations of (19) results in

$$-g_{tt}(r)g_{rr}(r)\dot{r}^2 + \mathcal{V}(\varepsilon, L, r) = E^2 \quad (21)$$

with the effective potential

$$\mathcal{V}(\varepsilon, L, r) = -g_{tt}(r) \left(\frac{L^2}{g_{\varphi\varphi}(r)} + \varepsilon \right). \quad (22)$$

Circular geodesics have to satisfy $\dot{r} = 0$ and $\ddot{r} = 0$, hence

$$\mathcal{V}(\varepsilon, L, r) = E^2, \quad \frac{\partial \mathcal{V}(\varepsilon, L, r)}{\partial r} = 0. \quad (23)$$

For lightlike geodesics, $\varepsilon = 0$, these two conditions are equivalent to

$$\frac{L^2}{E^2} = \frac{g_{\varphi\varphi}(r)}{-g_{tt}(r)}, \quad g_{tt}(r)g'_{\varphi\varphi}(r) = g_{\varphi\varphi}(r)g'_{tt}(r), \quad (24)$$

where a prime denotes derivative with respect to r . Comparison with (8) demonstrates that circular lightlike geodesics (“photon circles”) are located precisely at those points in the r - ϑ -plane where the differential of the von Zeipel radius \mathcal{R} vanishes.

For timelike geodesics, $\varepsilon = 1$, solving the two equations (23) for L and E gives us the so-called *Keplerian*[‡] values of these constants of motion,

$$L_K(r)^2 = \frac{g_{\varphi\varphi}(r)^2 g'_{tt}(r)}{g_{tt}(r) g'_{\varphi\varphi}(r) - g_{\varphi\varphi}(r) g'_{tt}(r)} \quad (25)$$

and

$$E_K(r)^2 = \frac{-g_{tt}(r)^2 g'_{\varphi\varphi}(r)}{g_{tt}(r) g'_{\varphi\varphi}(r) - g_{\varphi\varphi}(r) g'_{tt}(r)}. \quad (26)$$

Their quotient is the *Keplerian specific angular momentum*

$$l_K(r)^2 = \frac{L_K(r)^2}{E_K(r)^2} = \frac{-g_{\varphi\varphi}(r)^2 g'_{tt}(r)}{g_{tt}(r)^2 g'_{\varphi\varphi}(r)} = \frac{-(g^{tt})'(r)}{(g^{\varphi\varphi})'(r)}. \quad (27)$$

Analogously, evaluating the angular velocity $\Omega = \dot{\varphi}/\dot{t}$ along circular timelike geodesics gives the *Keplerian angular velocity*

$$\Omega_K(r)^2 = \left(\frac{g_{tt}(r) L_K(r)}{g_{\varphi\varphi}(r) E_K(r)} \right)^2 = \frac{-g'_{tt}(r)}{g'_{\varphi\varphi}(r)}. \quad (28)$$

A timelike circular geodesic is stable with respect to radial perturbations if it is a local minimum of \mathcal{V} , and is unstable if it is a local maximum. For distinguishing these cases, we assume that (23) holds with $\varepsilon = 1$ and calculate

$$\left. \frac{\partial^2 \mathcal{V}(1, L, r)}{\partial r^2} \right|_{L=L_K(r)} = -E_K(r)^2 g_{tt}(r) \left((g^{tt})''(r) + l_K(r)^2 (g^{\varphi\varphi})''(r) \right). \quad (29)$$

This demonstrates that a circular timelike geodesic at radius r is stable if the right-hand side of Eq. (29) is positive, and unstable if it is negative. This observation has an important consequence in view of the construction of Polish doughnuts. If we assume that Eq. (15) is satisfied, comparison of Eqs. (27) and (29) with (16) and (17) show the following: Every circular timelike geodesic in the equatorial plane gives a critical point of the potential \mathcal{W} . If the geodesic is stable with respect to radial perturbations, this critical point is a minimum of \mathcal{W} ; if the geodesic is unstable, it is a saddle. This implies in particular that Polish doughnuts can exist only around a stable timelike circular geodesic that serves as the centre.

In this paper, we are interested in spacetimes that are asymptotically flat with a positive ADM mass M_0 . Then we have $-g_{tt}(r) = 1 - 2M_0/r + \mathcal{O}((M_0/r)^2)$ with $M_0 > 0$ and $g_{\varphi\varphi}(r)/r^2 \rightarrow 1$ for $r \rightarrow \infty$. In this situation, the effective potential $\mathcal{V}(1, L, r)$ approaches the value 1 from below for $r \rightarrow \infty$. This implies that, for sufficiently big r , circular timelike geodesics are stable. At a certain radius $r = r_{\text{ms}}$ they may become unstable. At this radius, the right-hand side of (29) must be zero, i.e.

$$l_K(r_{\text{ms}})^2 = \frac{-(g^{tt})''(r_{\text{ms}})}{(g^{\varphi\varphi})''(r_{\text{ms}})}. \quad (30)$$

[‡] When referring to general-relativistic orbits, the attribute “Keplerian” means “relating to timelike circular geodesics”.

By (27), this condition is equivalent to

$$l'_K(r_{\text{ms}}) = 0. \quad (31)$$

Eq. (31) is the defining equation of a *marginally stable* circular orbit. Note that there may be more than one marginally stable orbit, i.e., when moving inwards we may encounter again stable orbits after having crossed a region with unstable ones.

If we have passed the first marginally stable orbit, coming from $r = \infty$, we are in a region where $\mathcal{V}(1, L_K(r), r) < 1$, implying that a perturbation of an unstable circular orbit in this region gives a bound orbit, i.e., an orbit that does not escape to infinity. The last circular timelike geodesic where this holds true is called the *marginally bound* orbit. Its radius r_{mb} must satisfy the equation $\mathcal{V}(1, L_K(r_{\text{mb}}), r_{\text{mb}}) = 1$, which can also be rewritten as

$$E_K(r_{\text{mb}})^2 = 1. \quad (32)$$

3. Tori in the q -metric

The most general axisymmetric and static solution of the vacuum field equations is represented by the Weyl class of solutions. The simplest of these solutions is the Schwarzschild metric, for which all multipole moments but the monopole moment (ADM mass) vanish. By the Jebsen-Birkhoff theorem, there is no other Weyl solution for which all the higher-order multipole moments vanish. Among the many different Weyl solutions with a non-vanishing quadrupole moment, the so-called q -metric is considered the simplest one. It can be written as

$$g_{\mu\nu}dx^\mu dx^\nu = -\left(1 - \frac{2M}{r}\right)^{1+q} dt^2 + \left(1 - \frac{2M}{r}\right)^{-q} \left[\left(1 + \frac{M^2 \sin^2 \vartheta}{r^2 - 2Mr}\right)^{-q(2+q)} \left(\frac{dr^2}{1 - \frac{2M}{r}} + r^2 d\vartheta^2 \right) + r^2 \sin^2 \vartheta d\varphi^2 \right] \quad (33)$$

where M is a parameter with the dimension of a length and q is a dimensionless parameter. We refer to M as to the mass parameter and to q as to the quadrupole parameter. In the representation given here, with the quadrupole parameter q , the metric (33) was found by Quevedo [4], cf. Quevedo et al. [7]. In other representations, this solution to the Einstein vacuum field equation was known before; it is a special case of a class of metrics discussed by Bach [8] and it was also studied e.g. by Zipoy [9] and Vorhees [10]. We also mention that Toktarbay and Quevedo [11] found a rotating (non-static) generalisation of the q -metric which, however, will not be considered in the following.

For $q = 0$ the q -metric reduces to the spherically symmetric Schwarzschild metric with ADM mass M . For $q = -2$ it also reduces to the Schwarzschild metric, as can be seen by transforming the radius coordinate according to $r \mapsto r - 2M$; this time, however, the ADM mass is equal to $-M$ if we define it, as usual, at $r = +\infty$. For any values of q and M the q -metric is symmetric with respect to the equatorial plane $\vartheta = \pi/2$

and asymptotically flat. For $M = 0$ and any value of q , it is flat. The same is true for $q = -1$ and any value of M , which is less obvious. In the case $M > 0$ and $q \neq -1$, the metric (33) is singular at the positive radius value $r = 2M$. While in the Schwarzschild case $q = 0$ this is a mere coordinate singularity, indicating a horizon, there is a naked curvature singularity at $r = 2M$ for all other values of q . As naked singularities are widely believed to be unphysical, it is reasonable to consider the q -metric only outside of a closed surface \mathcal{S} that surrounds the naked singularity, and to think of an interior matter solution being matched to this metric at \mathcal{S} , see Stewart et al. [12] and Quevedo et al. [7]. With this interpretation, the q -metric describes the gravitational field outside of a deformed celestial body that might be quite compact, but not compact enough to form a black hole.

The Geroch-Hansen mass monopole and quadrupole moments of the q -metric can be expressed as [4]

$$M_0 = (1 + q)M, \quad M_2 = -\frac{M^3}{3}q(1 + q)(2 + q). \quad (34)$$

All even multipole moments are different from zero and determined by M and q .

As we want the ADM mass M_0 to be positive, we have to choose either $M > 0$ and $q > -1$ or $M < 0$ and $q < -1$. Actually, it suffices to consider the first case. The reason is that the q -metric with parameters M and q is isometric to the q -metric with parameters $M' = -M$ and $q' = -q - 2$, as can be seen by transforming the radius coordinate according to $r \mapsto r' = r - 2M$. Therefore, the q -metrics with $M > 0$ and $q > -1$ are the same as the ones with $M' < 0$ and $q' < -1$.

From now on we assume that $M > 0$ and $q > -1$. For negative values of $q > -1$, the mass quadrupole moment M_2 is positive; the latter property means that, far away from the centre, the two-dimensional surfaces ($g_{tt} = \text{const.}, t = \text{const.}$) are prolate spheroids. They are oblate spheroids for positive values of q , which corresponds to negative values of M_2 , cf. Quevedo et al. [7, 13].

For better comparison with other (quadrupolar) spacetimes, it is convenient to express the q -metric in terms of M_0 and M_2 , rather than in terms of M and q . The transformation $(M_0, M_2) \mapsto (M, q)$ is given by:

$$M = M_0 \sqrt{3 \frac{M_2}{M_0^3} + 1}, \quad q = \frac{1}{\sqrt{3 \frac{M_2}{M_0^3} + 1}} - 1. \quad (35)$$

Demanding the expression under the root to be positive, resulting in a real (and positive) M , requires $M_2/M_0^3 > -1/3$. In other words, in the oblate case the values of M_2 are restricted once M_0 has been chosen. We will see below that there is no such restriction for the Erez-Rosen metric.

For later convenience we also mention that the Kretschmann scalar of the q -metric can be expressed as [14]

$$\mathcal{K} = R_{\beta\gamma\delta\eta}R^{\beta\gamma\delta\eta} = \frac{16M^2(1 + q)^2(r^2 - 2Mr + M^2 \sin^2 \vartheta)^{2(2q+q^2)-1}}{r^{4(2+2q+q^2)}(1 - 2M/r)^{2(q^2+q+1)}} \mathcal{F}(r, \vartheta) \quad (36)$$

with

$$\begin{aligned}\mathcal{F}(r, \vartheta) = & 3(r - 2M - qM)^2(r^2 - 2Mr + M^2 \sin^2 \vartheta) \\ & + M^2 q(2 + q) \sin^2 \vartheta [M^2 q(2 + q) + 3(r - M)(r - 2M - qM)].\end{aligned}\quad (37)$$

In the Schwarzschild case $q = 0$, the Kretschmann scalar reduces to $\mathcal{K} = 48M^2/r^6$, being regular at $r = 2M$. For all other values of $q(> -1)$, the Kretschmann scalar diverges at $r = 2M$, indicating a curvature singularity.

3.1. Lightlike and timelike circular geodesics

Next, lightlike and timelike circular geodesics in the equatorial plane are briefly discussed. For the q -metric, the effective potential (22) specifies to

$$\mathcal{V} = \left(1 - \frac{2M}{r}\right)^{q+1} \left[\frac{L^2}{r^2} \left(1 - \frac{2M}{r}\right)^q + \varepsilon \right] \quad (38)$$

For lightlike geodesics ($\varepsilon = 0$), the conditions (23) for circular orbits admit exactly one solution for the radius

$$r_c = (3 + 2q)M = \left(2 + \sqrt{1 + 3\frac{M_2}{M_0^3}}\right)M_0 \quad (39)$$

and the specific angular momentum

$$\frac{L^2}{E^2} = \frac{r_c^2}{\left(1 - \frac{2M}{r_c}\right)^{1+2q}}. \quad (40)$$

Thus, a photon circle exists in the region outside the singularity if $q > -1/2$. This photon circle is unstable with respect to radial perturbations. In the Schwarzschild limit $q \rightarrow 0$, (39) and (40) reduce to the well-known values $r_c = 3M$ and $L^2/E^2 = 27M^2$. For positive values of q (negative values of M_2/M_0^3), the radius r_c is greater than $3M$ and approaches infinity for $q \rightarrow \infty$; for negative values of q (positive values of M_2/M_0^3), it is smaller than $3M$ and approaches the singularity at $2M$ for $q \rightarrow -1/2$. For a plot of r_c as a function of the quadrupole moment, see figure 1.

For timelike geodesics ($\varepsilon = 1$), the conditions (23) for circular orbits result in the Keplerian values

$$L_K(r)^2 = \left(1 - \frac{2M}{r}\right)^{-q} \frac{(1 + q)Mr^2}{r - (3 + 2q)M} \quad (41)$$

and

$$E_K(r)^2 = \left(1 - \frac{2M}{r}\right)^{1+q} \frac{r - (2 + q)M}{r - (3 + 2q)M}. \quad (42)$$

As $L_K(r)^2$ cannot be negative, circular timelike geodesics exist for $r > r_c$ where r_c is the radius of the unstable circular lightlike geodesic given in (39).

From $L_K(r)$ and $E_K(r)$ we find the Keplerian specific angular momentum

$$l_K(r)^2 = \left(1 - \frac{2M}{r}\right)^{-(1+2q)} \frac{(1 + q)Mr^2}{r - (2 + q)M} \quad (43)$$

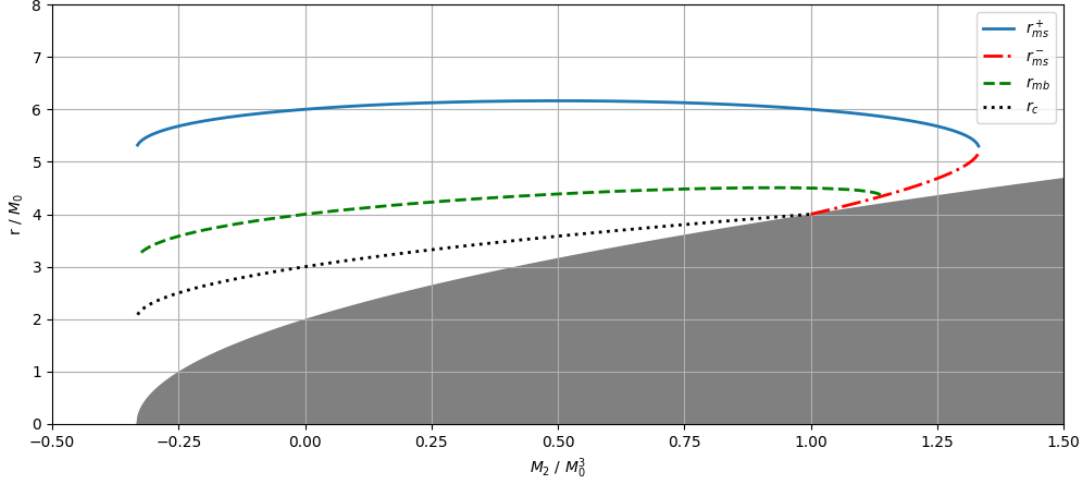


Figure 1. Circular equatorial geodesics in the q -metric, depending on the mass quadrupole moment M_2/M_0^3 . Note that $q \rightarrow \infty$ corresponds to $M_2/M_0^3 = -1/3$, and $q = -1$ corresponds to $M_2/M_0^3 \rightarrow \infty$. Blue solid line: positive solution of the marginally stable circular orbit r_{ms}^+ ; red dash-dotted line: negative solution of the marginally stable circular orbit r_{ms}^- ; green dashed line: marginally bound circular orbit r_{mb} ; black dotted line: photon circle r_c . The grey shaded area marks the region inside the naked singularity, $r \leq 2M$.

and, with (28), the Keplerian angular velocity

$$\Omega_K(r)^2 = \left(1 - \frac{2M}{r}\right)^{1+2q} \frac{(1+q)M}{r^2(r - (2+q)M)}. \quad (44)$$

For determining the marginally bound orbits, we have to solve the equation $E_K(r)^2 = \mathcal{V}(1, L_K(r), r) = 1$ for r . This cannot be done analytically, thus r_{mb} is only computed numerically. The result is depicted in figure 1.

The marginally stable circular orbits in the q -metric have been calculated already by Boshkayev et.al. [15]. In general, there are two of them, an inner one at $r = r_{\text{ms}}^-$ and an outer one at $r = r_{\text{ms}}^+$, where

$$r_{\text{ms}}^\pm = M \left(4 + 3q \pm \sqrt{5q^2 + 10q + 4} \right). \quad (45)$$

This result can easily be verified by solving the equation (31). When evaluating Eq. (45), one has to keep in mind that $q > -1$ and $r > r_c$. These restrictions divide the family of q -metrics into three classes:

Class I : $\infty > q > -1/2$, i.e. $-1/3 < M_2/M_0^3 < 1$

In this class, there is only one marginally stable orbit at r_{ms}^+ . Orbits between r_{ms}^+ and infinity are stable, whereas orbits between r_c and r_{ms}^+ are unstable. Between $2M$ and r_c , there are no circular timelike geodesics. For $q \rightarrow -1/2$, we find $r_{\text{ms}}^+/M \rightarrow 3$, which corresponds to $r_{\text{ms}}^+/M_0 \rightarrow 6$, and for $q \rightarrow \infty$ we find $r_{\text{ms}}^+/M \rightarrow \infty$ which corresponds to $r_{\text{ms}}^+/M_0 \rightarrow 3 + \sqrt{5}$.

Class II : $-1/2 > q > -1 + 1/\sqrt{5} \approx -0.553$, i.e., $1 < M_2/M_0^3 < 4/3$

In this class, there are two marginally stable circular orbits at r_{ms}^\pm . In the interval $r_{\text{ms}}^- < r < r_{\text{ms}}^+$ circular orbits are unstable, for radii $r > r_{\text{ms}}^+$ and $2M < r < r_{\text{ms}}^-$, they are stable. In the limiting case $q \rightarrow -1 + 1/\sqrt{5}$, the two marginally stable orbits merge at $r_{\text{ms}}^\pm = (1 + 3/\sqrt{5})M = (3 + \sqrt{5})M_0$.

Class III : $-1 + 1/\sqrt{5} > q > -1$, i.e., $4/3 < M_2/M_0^3 < \infty$

In this class, there are no marginally stable circular orbits. At any radius $r > 2M$ there is a stable circular timelike geodesic. Note that $l_K(r)^2 \rightarrow 0$ and $\Omega_K(r)^2 \rightarrow \infty$ for $r \rightarrow 2M$.

The radii of the photon circle, the marginally bound orbit and the marginally stable orbits, given in units of M_0 , are plotted in figure 1 against the quadrupole moment M_2/M_0^3 . The graphs of r_c , r_{mb} and r_{ms}^+ start at $M_2/M_0^3 = -1/3$, which corresponds to $q \rightarrow \infty$. The photon radius r_c increases monotonically, but drops under the position of the singularity at $M_2/M_0^3 = 1$, corresponding to $q = -1/2$. Above this value of M_2/M_0^3 , there are two marginally stable circular orbits which merge at $M_2/M_0^3 = 4/3$, and then vanish. Between the photon orbit and the marginally stable orbit, the marginally bound circular orbit can be found; it vanishes above $M_2/M_0^3 \approx 1.13$, where the maximum of \mathcal{V} drops below 1.

Inserting the radius values r_{ms}^\pm and r_{mb} into (43) gives the specific angular momentum of the marginally stable and marginally bound orbits, which we denote by l_{ms}^\pm and l_{mb} , respectively. In figure 2, we show plots of l_{ms}^\pm and l_{mb} , depending on the quadrupole moment.

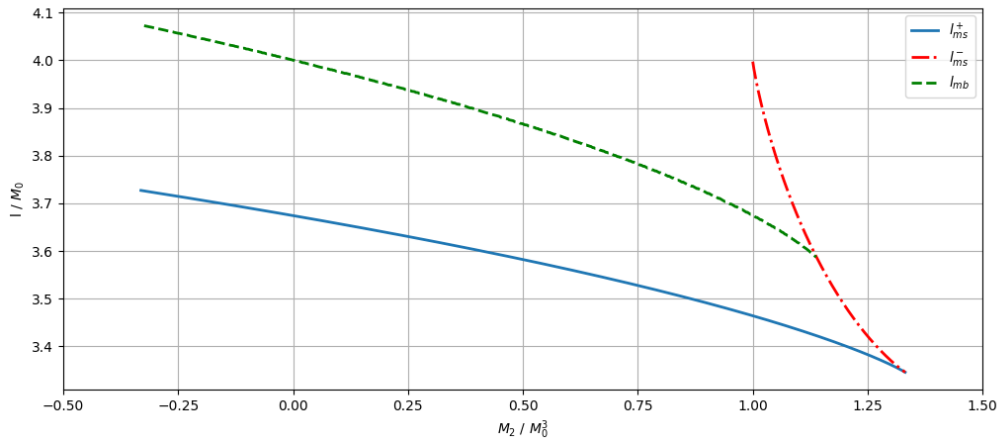


Figure 2. Specific angular momentum of the marginally stable orbits (blue solid and red dash-dotted lines) and of the marginally bound orbits (green dashed line) in the q -metric, depending on the mass monopole moment M_2/M_0^3 .

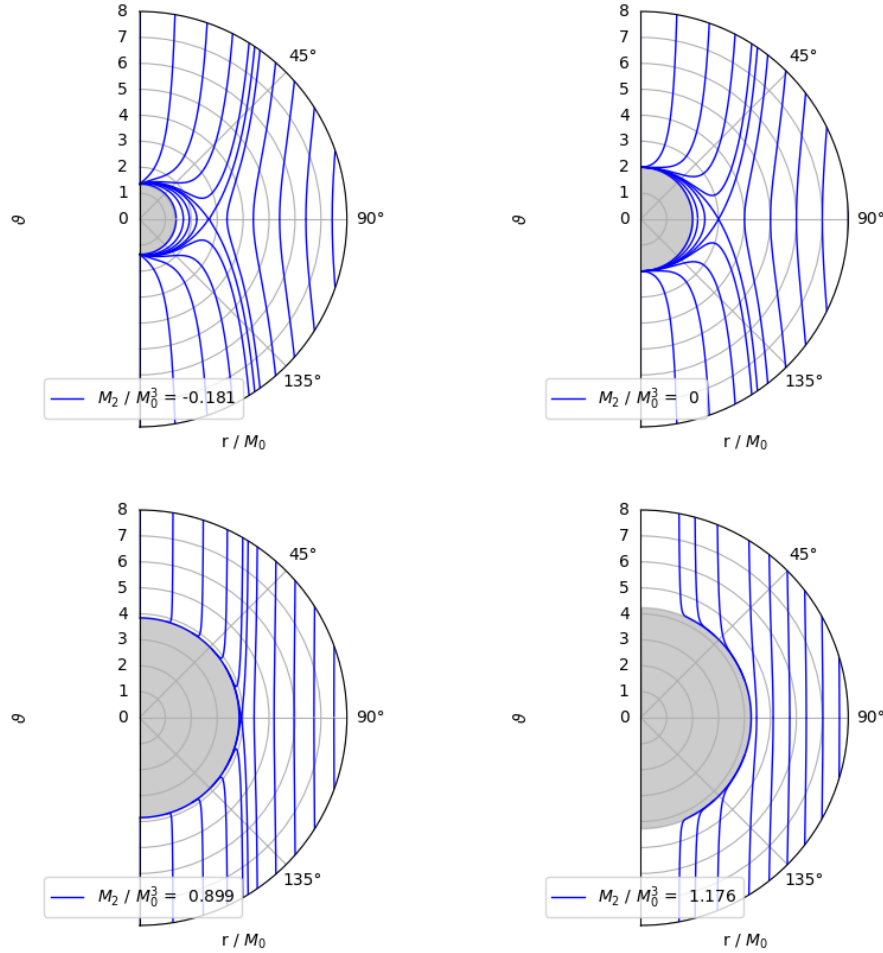


Figure 3. Von Zeipel cylinders for different mass quadrupole moments in the q -metric. Upper-left: von Zeipel cylinders for negative values of M_2/M_0^3 , corresponding to an oblate geometry; upper-right: von Zeipel cylinders for vanishing quadrupole moment, corresponding to the Schwarzschild limit; lower-left: von Zeipel cylinders for positive values of M_2/M_0^3 , corresponding to a prolate geometry; lower-right: von Zeipel cylinders for M_2/M_0^3 in Case II - here, there is no crossing surface anymore, as there is no photon circle. The grey-shaded areas indicate the area below the singularity $r \leq 2M$.

3.2. Von Zeipel cylinders

In this section, the von Zeipel cylinders are calculated in the q -metric. They give an insight into the behaviour of circular motions in this metric. Recall that, for any static and axisymmetric spacetime, these cylinders are independent of the specific angular momentum.

The von Zeipel cylinders are defined as the surfaces $\mathcal{R} = \text{const.}$ with \mathcal{R} given by (8). In the q -metric, this reduces to

$$\mathcal{R}(r, \vartheta)^2 = \frac{\left(1 - \frac{2M}{r}\right)^{1+2q}}{r^2 \sin^2 \vartheta}. \quad (46)$$

The surfaces $\mathcal{R} = \text{const.}$ are plotted in figure 3 for different quadrupole moments M_2/M_0^3 . Note that, according to (24), the differential $d\mathcal{R}$ has a zero at the photon circle ($r = r_c, \vartheta = \pi/2$); the corresponding von Zeipel cylinder has a self-crossing there.

3.3. Effective potential

For constructing Polish doughnuts, we calculate the effective potential (12) for the q -metric:

$$\mathcal{W}(l, r, \vartheta) = \frac{1}{2} \ln \left[\frac{r^2 \sin^2 \vartheta}{\left(1 - \frac{2M}{r}\right)^{-(1+q)} r^2 \sin^2 \vartheta - l^2 \left(1 - \frac{2M}{r}\right)^q} \right]. \quad (47)$$

In figure 4 we plot this potential restricted to the equatorial plane as a function of the radius coordinate, for various values of M_2 and l with M_0 chosen as the unit of length. In figures 5 and 6 we show the equipotential surfaces $\mathcal{W} = \text{const.}$ in the r - ϑ -plane, again for various values of M_2 and l . For the boundary of the torus, we may choose any closed equipotential surface. We indicate the maximal torus for a given l by a blue-shaded area; this maximal domain is known as the *Roche lobe*. Recall that the equipotential surfaces and, consequently the shape of the torus, is independent of the parameters that enter into the equation of state. We have also calculated the density ρ , which does depend on the equation of state. In figures 5 and 6, we give the density ρ/M_0^2 , where we have assumed a particular polytropic equation of state, as explained in section 2.

We will now discuss the properties of the Polish doughnuts in the q -metric and the differences to the Schwarzschild case in detail. We recall that, for the construction of the accretion tori, we need a stable circular timelike geodesic in the equatorial plane that can serve as the centre. The region where such orbits occur depends on the class of q -metrics described above. Thus, the three classes are discussed individually. Note that in *any* case the potential \mathcal{W} goes to 0 from below for $r \rightarrow \infty$.

We begin with Class I, which contains the Schwarzschild spacetime as a special case. Here, we have a photon circle at radius r_c , a marginally bound orbit at radius r_{mb} and exactly one marginally stable orbit at r_{ms}^+ , where $2M < r_c < r_{\text{mb}} < r_{\text{ms}}^+ < \infty$. For the construction of the torus, one chooses l such that $l^2 > (l_{\text{ms}}^+)^2$; this guarantees the existence of a centre. Then the potential \mathcal{W} features a local minimum at some radius r_{cen} , and a local maximum at some radius r_{cusp} , where $r_{\text{cusp}} < r_{\text{cen}}$; the potential goes to $-\infty$ for $r \rightarrow 2M$, see the first three panels of figure 4 for examples. Following the definition of the marginally bound orbit, it follows that $\mathcal{W}(l, r_{\text{cusp}}, \pi/2) < 0$ as long as $l^2 < l_{\text{mb}}^2$. In that case, we get a closed equipotential surface by choosing \mathcal{W}_{in} such that $\mathcal{W}(l, r_{\text{cen}}, \pi/2) < \mathcal{W}_{\text{in}} \leq \mathcal{W}(l, r_{\text{mb}}, \pi/2)$. The maximal volume the fluid can occupy without overflowing is reached by choosing $\mathcal{W}_{\text{in}} = \mathcal{W}(l, r_{\text{mb}}, \pi/2)$; we have already mentioned that this volume is called the “Roche lobe”. The suffix “cusp” in r_{cusp}

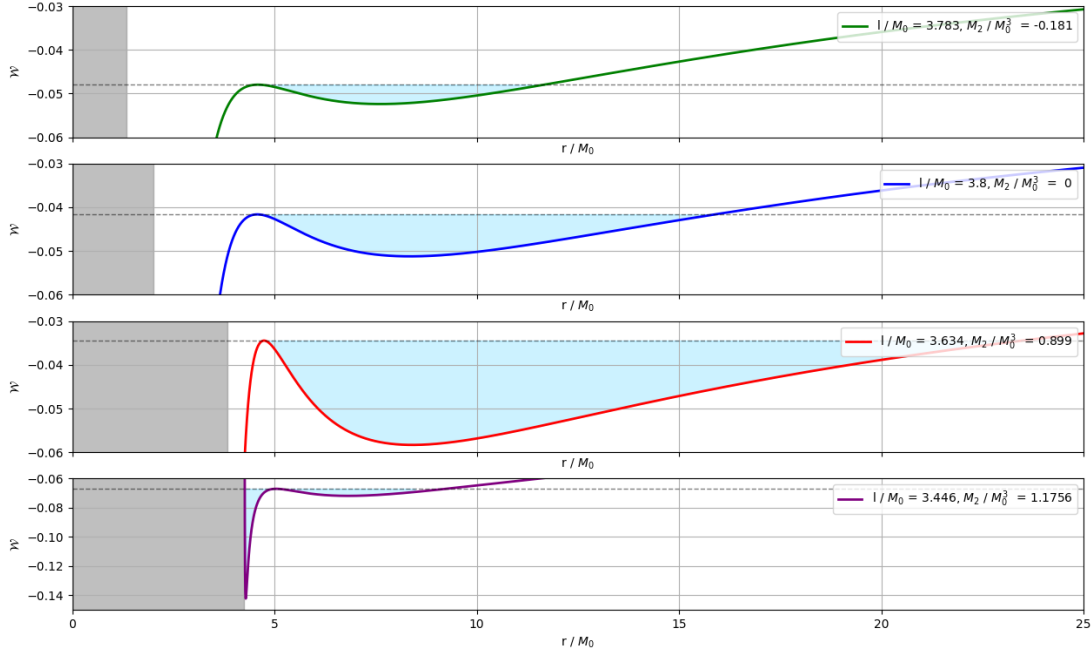


Figure 4. Effective potential in the equatorial plane in the q -metric, depending on M_2/M_0^3 . The grey shaded area indicates the region bounded by the singularity, the lighter blue-shaded area is the region occupied by a torus that fills its Roche lobe completely. Upper graph: Class I spacetime with a negative value of M_2/M_0^3 , corresponding to an oblate geometry; upper-middle graph: Schwarzschild spacetime; lower-middle graph: Class I spacetime with a positive value of M_2/M_0^3 , corresponding to a prolate geometry; lower graph: Class II spacetime, note that effective potential approaches $+\infty$ for $r \rightarrow r_{\text{sing}}$.

refers to the fact that the Roche lobe features a cusp at $(r = r_{\text{cusp}}, \vartheta = \pi/2)$. In figure 5, we show three such tori that fill their Roche lobes completely, restricted to the equatorial plane. Tori that fill their Roche lobes completely are of particular interest because the fluid is at the verge of overflowing towards the centre; in this sense, such stationary rotating tori approximate fluid configurations with an accretion flow onto the central object. For constructing Polish doughnuts, we may also choose $l^2 > l_{\text{mb}}^2$. Then \mathcal{W}_{in} is limited by $\mathcal{W}_{\text{in}} < 0$, as otherwise the torus would extend to infinity. Such a Polish doughnut does not feature a cusp at its inner edge, so it is not at the verge of accretion. For this reason, tori with $(l_{\text{mb}}^+)^2 < l^2 < l_{\text{mb}}^2$ are usually considered as being more interesting.

We now turn to spacetimes of Class II, which show considerably different qualitative features. In this case there are two marginally stable orbits and, potentially, one marginally bound orbit in the unstable region between them, $2M < r_{\text{ms}}^- (< r_{\text{mb}}) < r_{\text{ms}}^+ < \infty$. Qualitatively different types of Polish doughnuts exist for $l^2 > (l_{\text{ms}}^+)^2$. Here, the potential $\mathcal{W}(l, r, \pi/2)$ has two minima at $r_{\text{cen},1}$ and $r_{\text{cen},2}$, and a maximum at r_{cusp} ;

the effective potential goes to $+\infty$ at some radius r_s where $2M < r_s < r_{\text{cen},2} < r_{\text{cusp}} < r_{\text{cen},1} < \infty$, see the last panel of figure 4. Regardless of whether the marginally bound orbit exists, we may always choose l such that $\mathcal{W}(l, r_{\text{cusp}}, \pi/2) < 0$. If the marginally bound orbit exists, this can be achieved by choosing $(l_{\text{ms}}^+)^2 < l^2 < l_{\text{mb}}^2$; if it does not exist, any choice $(l_{\text{ms}}^+)^2 < l^2$ will do. In that case, the inequality $\mathcal{W}(l, r, \vartheta) \leq \mathcal{W}(l, r_{\text{cusp}}, \pi/2)$ defines *two* Roche lobes, both isolated from the singularity at $r = 2M$ and from infinity, touching at $(r = r_{\text{cusp}}, \vartheta = \pi/2)$. Perfect-fluid configurations in the form of double tori also exist in the Kerr spacetime, see Pugliese et al. [16, 17]. Double tori have also been found for *charged* fluids in the presence of a magnetic field in the Schwarzschild spacetime, see Trova et.al. [18]. However, they have not been observed before, to the best of our knowledge, for uncharged fluids on a static spacetime. In particular, such double tori cannot be constructed in the unperturbed Schwarzschild metric, or in any q -metric of Class I, irregardless of the choice of l . The last panel in figure 4 and figure 6 show such double tori. As one can see in figure 6, the cross-section of the Roche lobes has the shape of a fish§, with the outer lobe corresponding to the body of the fish and the inner lobe to the fish-tail. The major difference of figure 6 in comparison to figure 5 is in the fact that the “fish-tail” is isolated from the singularity, i.e., we can match at a surface \mathcal{S} an interior solution to the q -metric in such a way that the inner torus does not touch \mathcal{S} . Note that in such double-torus configurations the inner and the outer torus could rotate in opposite directions if they do not fill their Roche lobes completely. As the inner Roche lobe has no cusp at its *inner* edge, these double tori are not at the verge of accretion. Correspondingly, if the two tori are bigger than their Roche lobes, the fluid will not spill over towards the centre or towards infinity; it will rather form a single torus, without cusps, but with two centres; such a double-centre torus can be constructed, with the same l as the double tori, by choosing \mathcal{W}_{in} such that $\mathcal{W}(l, r_{\text{cusp}}, \pi/2) < \mathcal{W}_{\text{in}} < 0$, see the picture on the left in figure 6. This corresponds to raising the dashed line in the lowermost panel of figure 4.

In spacetimes of Class III, there is a stable circular orbit at any radius $r > 2M$. Each of these orbits can be chosen as the centre of a Polish doughnut. However, as there are no unstable circular orbits, no cusp exists, i.e., the Polish doughnuts in such a spacetime can never be at the verge of accretion. All tori in this class are qualitatively similar to the tori with $l^2 > l_{\text{mb}}^2$ constructed in the Schwarzschild spacetime.

Note that we have assumed that the spacetime geometry is given by the unperturbed q -metric, i.e., we have neglected the influence of the mass of the fluid on the spacetime. This assumption is justified as long as the density of the fluid is sufficiently small. For the numerical examples shown in figure 5, we demonstrate in the caption that the density squared at the centre of the torus is much smaller than the Kretschmann scalar at this point, demonstrating that the torus has a negligible effect on the spacetime geometry.

§ *Polish Fishes*, as one might call them

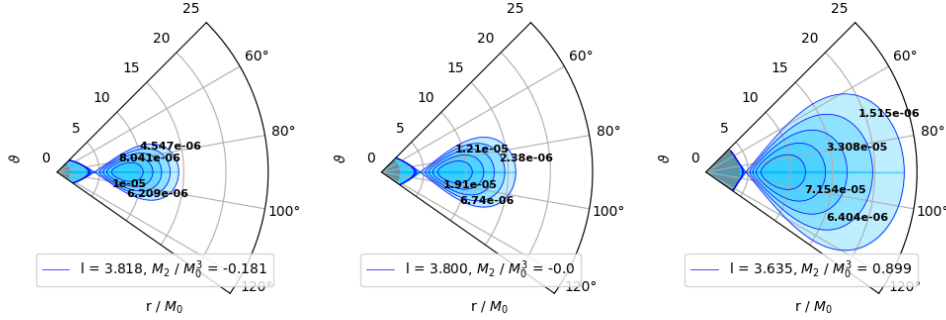


Figure 5. Polar dependency of the effective potential in the q -metric. The black numbers represent the density in units of M_0^{-2} , assuming a polytropic equation of state with $K = 0.2$ and $\Gamma = 5/3$. We compare the density ρ with the Kretschmann scalar \mathcal{K} at the centre to demonstrate that the gravitative influence of the fluid is negligible. Left: torus in a Class I spacetime with a negative value of M_2/M_0^3 , corresponding to an oblate geometry, $\rho(r_{\text{cen}})^2/\mathcal{K}(r_{\text{cen}}) = 3.528 \times 10^{-6}$; middle: torus in the Schwarzschild spacetime, $\rho(r_{\text{cen}})^2/\mathcal{K}(r_{\text{cen}}) = 1.18 \times 10^{-6}$; right: torus in a Class I spacetime with a positive value of M_2/M_0^3 , corresponding to a prolate geometry, $\rho(r_{\text{cen}})^2/\mathcal{K}(r_{\text{cen}}) = 9.389 \times 10^{-8}$.

4. Tori in the Erez-Rosen spacetime

Next, we consider the *Erez-Rosen* metric, which is a static and axisymmetric solution to Einstein's vacuum field equation that was found by Erez and Rosen in 1959 [5]. It was the first metric found in the class of Weyl solutions that was identified as describing the gravitational field around a central object with a quadrupole moment. For the correction of several misprints in the original paper by Erez and Rosen, we refer to Young and Coulter [19].

The metric can be written in prolate spheroidal coordinates (t, φ, x, y) as

$$ds^2 = g_{\mu\nu}dx^\mu dx^\nu = -f(x, y)dt^2 + \frac{M^2}{f(x, y)} \left[e^{2\gamma(x, y)}(x^2 - y^2) \left(\frac{dx^2}{x^2 - 1} + \frac{dy^2}{1 - y^2} \right) + (x^2 - 1)(1 - y^2)d\varphi^2 \right] \quad (48)$$

where

$$f(x, y) = \frac{x - 1}{x + 1} e^{-2qP_2(y)Q_2(x)}, \quad (49)$$

$$\begin{aligned} \gamma(x, y) = & \frac{1}{2}(1 + q)^2 \ln \frac{x^2 - 1}{x^2 - y^2} + 2q(1 - P_2(y))Q_1(x) \\ & + q^2(1 - P_2(y)) \left[(1 + P_2(y))(Q_1(x)^2 - Q_2(x)^2) \right. \\ & \left. + \frac{1}{2}(x^2 - 1)(2Q_2(x)^2 - 3xQ_1(x)Q_2(x) + 3Q_0(x)Q_2(x) - Q_2'(x)) \right] \end{aligned} \quad (50)$$

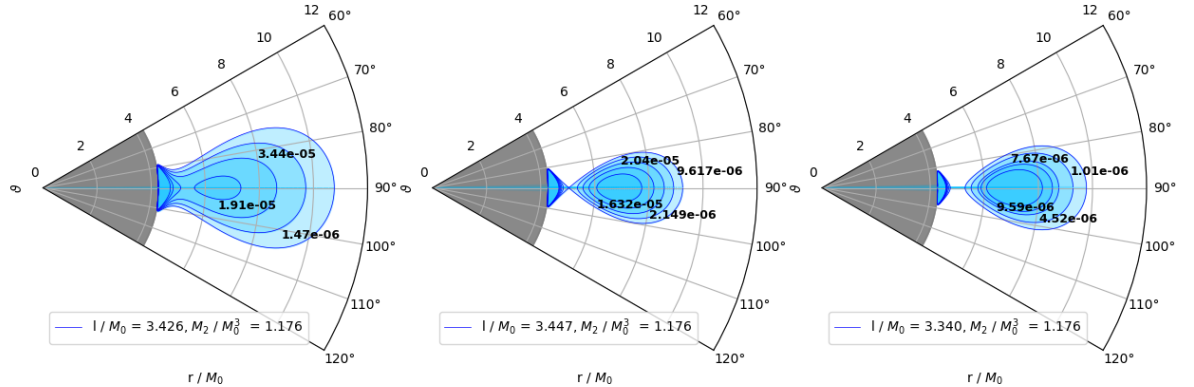


Figure 6. Polar dependency of the effective potential in the q -metric, for connected double tori (left panel), touching double tori (middle panel) and spatially separated tori (right panel), for a spacetime of Class II. The black numbers represent the density where we have assumed a polytropic equation of state with $K = 0.2$ and $\Gamma = 5/3$; left: $\rho^2(r_{\text{cen}})/\mathcal{K}(r_{\text{cen}}) = 1.78 \times 10^{-5}$, middle: $\rho^2(r_{\text{cen}})/\mathcal{K}(r_{\text{cen}}) = 1.04 \times 10^{-5}$, right: $\rho^2(r_{\text{cen}})/\mathcal{K}(r_{\text{cen}}) = 8.74 \times 10^{-6}$. Note that the inner Roche lobe is in close proximity to the singularity at $r = 2M$, but is indeed isolated from it.

The functions $P_l(y)$ and $Q_k(x)$ are the Legendre functions of first and second kind, respectively. Similarly to the q -metric, the Erez-Rosen metric depends on two parameters: A mass parameter M and a quadrupole parameter q . M has the dimension of a length, whereas q is dimensionless.

While the prolate spheroidal coordinates x and y are convenient for verifying that the metric satisfies the vacuum field equation, for comparing with the q -metric it is advisable to transform the metric into Schwarzschild-like coordinates by

$$x = \frac{r}{M} - 1, \quad y = \cos \vartheta. \quad (51)$$

In these coordinates $(t, \varphi, \vartheta, r)$ the metric was given in the original article by Erez and Rosen [5]. For a discussion of the timelike and lightlike geodesics in this vacuum spacetime we refer to Quevedo and Parkes [20]. We also mention that Castejon-Amenedo and Manko [21] have used the Erez-Rosen metric as a seed metric for constructing stationary (rotating) solutions to Einstein's vacuum field equation which, however, will not be considered in the following.

For $q = 0$, the Erez-Rosen metric reduces to the spherically symmetric Schwarzschild metric. Just as the q -metric, the Erez-Rosen metric is symmetric with respect to the equatorial plane $\vartheta = \pi/2$, and it is asymptotically flat for any values of (q, M) . For $M = 0$, irregardless of q , the spacetime becomes flat. If $M \neq 0$, the metric has a

singularity at $r = 2M$. In the Schwarzschild case, $q = 0$, this is a coordinate singularity, indicating a horizon. In any other case, $q \neq 0$, there is a naked curvature singularity at $r = 2M$. As in the case of the q -metric we may think of the Erez-Rosen metric as being valid only outside of a surface \mathcal{S} that surrounds the naked singularity, with an interior matter solution matched at \mathcal{S} . We may then interpret the Erez-Rosen spacetime as describing the gravitational field around a deformed, compact stellar object.

For the following calculations, the metric components g_{tt} and $g_{\varphi\varphi}$ are of importance. In the Schwarzschild-like coordinates, they read

$$g_{tt}(r, \vartheta) = -\left(1 - \frac{2M}{r}\right) e^{-2qP_2(\cos \vartheta)Q_2(r/M-1)} \quad (52)$$

$$g_{\varphi\varphi}(r, \vartheta) = r^2 \sin^2 \vartheta e^{2qP_2(\cos \vartheta)Q_2(r/M-1)} \quad (53)$$

with

$$P_2(\cos \vartheta) = \frac{1}{2}(3 \cos^2 \vartheta - 1), \quad (54)$$

$$Q_2(r/M - 1) = -\frac{1}{4}\left(\frac{3r^2}{M^2} - \frac{6r}{M} + 2\right) \ln\left(1 - \frac{2M}{r}\right) - \frac{3}{2}\left(\frac{r}{M} - 1\right). \quad (55)$$

The Geroch-Hansen mass monopole and quadrupole moments of the Erez-Rosen spacetime can be expressed as [22, 13]:

$$M_0 = M, \quad M_2 = \frac{2}{15}q^3 M^3 \quad (56)$$

We require again M_0 to be positive. In contrast to the q -metric, M_0 does not depend on the quadrupole parameter q ; thus, there is no restriction on q . For any positive value of M_0 , the quadrupole parameter q , and thereby M_2/M_0^3 , may take any value between $-\infty$ and ∞ . Moreover, it is important to notice that in the Erez-Rosen spacetime a positive value of q corresponds to a positive value of M_2 ; by contrast, in the q -metric (where we assumed $M > 0$ and $q > -1$ without loss of generality) q and M_2 had opposite signs.

The explicit form of the Kretschmann scalar of the Erez-Rosen metric will not be given here because of its very complicated structure, see Frutos-Alfaro et al. [14], Appendix B. In the Schwarzschild limit $q = 0$, the Kretschmann scalar reduces to the known expression of $\mathcal{K} = 48M^2/r^6$, which is regular at $r = 2M$. For any other value of q , the Kretschmann scalar diverges at $r = 2M$, indicating a curvature singularity. In this regard, the Erez-Rosen metric shows the same features as the q -metric.

4.1. Lightlike and timelike circular geodesics, marginally stable and marginally bound circular orbits

For the discussion of lightlike and timelike circular geodesics in the equatorial plane $\vartheta = \pi/2$, we insert (52) and (53) into (22) to get the effective potential

$$\mathcal{V}(\varepsilon, L, r) = \left(1 - \frac{2M}{r}\right) e^{qQ_2(r/M-1)} \left(\frac{L^2}{r^2} e^{qQ_2(r/M-1)} + \varepsilon\right) \quad (57)$$

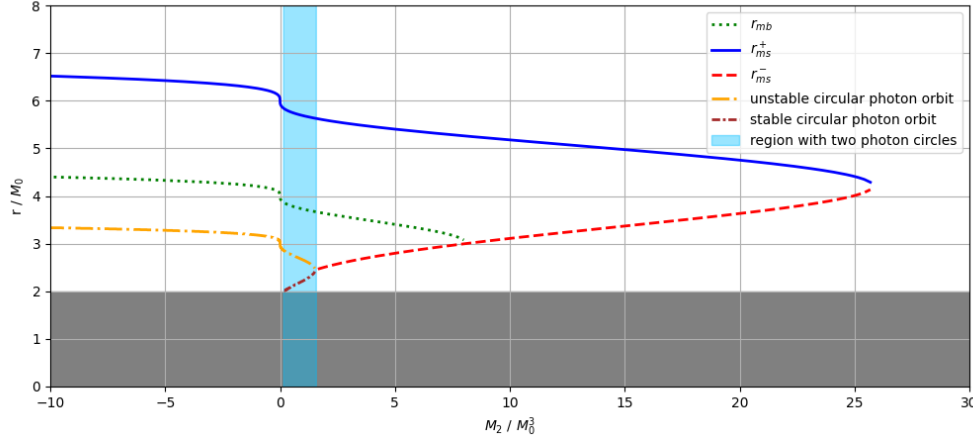


Figure 7. Circular equatorial geodesics in the Erez-Rosen spacetime, depending on the mass quadrupole moment M_2/M_0^3 . Blue solid and red dashed line: marginally stable circular orbit; green dotted line: marginally bound circular orbit; yellow and brown dash-dotted lines: positions of the photon circles.

where we used that $P_2(0) = -1/2$. If we insert this expression of the effective potential into (23), we get the equation for circular lightlike geodesics $\varepsilon = 0$ in the equatorial plane:

$$r - 3M + qr(r - 2M)u(r) = 0 \quad (58)$$

where

$$u(r) := \frac{d}{dr}Q_2(r/M - 1) = -\frac{3}{M} - \frac{M}{r(r - 2M)} - \frac{3(r - M)}{2M^2} \ln\left(1 - \frac{2M}{r}\right). \quad (59)$$

There are at most two solutions of this equation which we denote $r = r_c^+$ and $r = r_c^-$; however, it depends on the value of q whether they lie outside of the singularity. For $q \leq 1$ (corresponding to $M_2/M_0^3 \lesssim 0.13$), there is only one photon circle, at a radius $r = r_c^+$; this photon circle is unstable. In the Schwarzschild limit $q = 0$, we get again the familiar value of $r_c^+ = 3M$. In the limiting case $q \rightarrow -\infty$, equivalent to $M_2/M_0^3 \rightarrow -\infty$, we have $r_c^+ \rightarrow \infty$, whereas in the other limiting case $q = 1$, we have $r_c^+ \approx 2.87M$. For $1 < q \lesssim 2.25$, corresponding to $0.13 \lesssim M_2/M_0^3 \lesssim 1.52$, there exist two photon circles at radii r_c^+ and r_c^- . The inner one at r_c^- is stable, while the outer one at r_c^+ is unstable. Beyond $q \approx 2.25$, there is no photon circle anymore. The positions of the photon circles are plotted in figure 7.

For timelike geodesics ($\varepsilon = 1$), the conditions (23) for circular orbits give the following expressions for the Keplerian values:

$$L_K(r)^2 = \frac{e^{-qQ_2(r/M-1)} r^2 \left(2M + (r - 2M) q r u(r) \right)}{2 \left(r - 3M - (r - 2M) q r u(r) \right)} \quad (60)$$

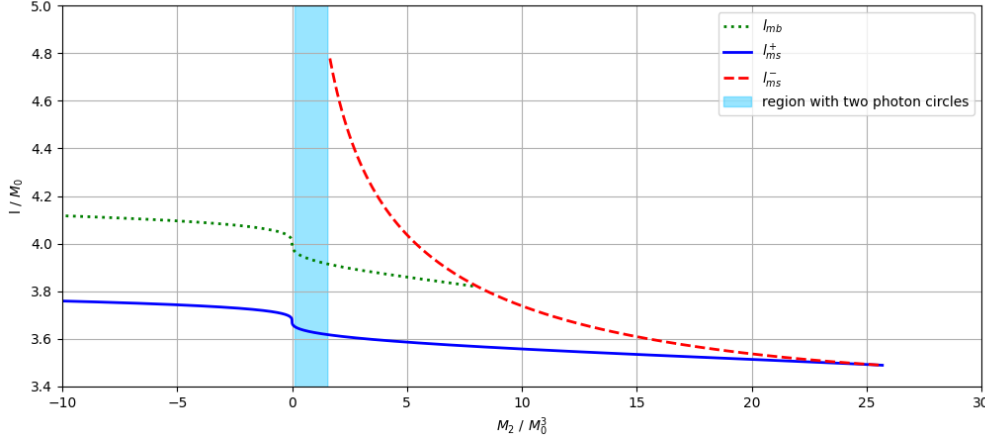


Figure 8. Specific angular momentum of the marginally stable (blue solid and red dashed lines) and marginally bound orbits (green dotted line) in the Erez-Rosen spacetime, depending on the quadrupole moment M_2/M_0^3 .

and

$$E_K(r)^2 = \frac{e^{qQ_2(r/M-1)}(r-2M)^2(2-qu(r))}{2r(r-3M-(r-2M)qu(r))} \quad (61)$$

From $L_K(r)$ and $E_K(r)$, we can find the Keplerian specific angular momentum

$$l_K(r)^2 = \frac{e^{-2qQ_2(r/M-1)}r^3(2M+(r-2M)qu(r))}{(r-2M)^2(2-qu(r))} \quad (62)$$

and the Keplerian angular velocity

$$\Omega_K(r)^2 = \frac{e^{2qQ_2(r/M-1)}(2M+(r-2M)qu(r))}{r^3(2-qu(r))}. \quad (63)$$

Following these equations, we can calculate the marginally stable orbits r_{ms} and marginally bound orbit $r = r_{\text{mb}}$, with the help of (31) and (32), respectively. The calculation can be done only numerically in both cases. We find the existence of at most two marginally stable orbits, at radii r_{ms}^+ and r_{ms}^- , and of at most one marginally bound orbit, at radius r_{mb} . In figure 7, the position of the marginally stable and marginally bound orbits are depicted, along with the position of the photon circles, depending on the quadrupole moment. In this figure, we plot on the vertical axis all radius values in units of the mass monopole moment M_0 , and on the horizontal axis the quadrupole moment in terms of the asymptotically and invariantly defined quantity M_2/M_0^3 . In this way, the plots for the Erez-Rosen spacetime are directly comparable to the plots for the q -metric. Note that in this diagram M_2/M_0^3 ranges from $-\infty$ to ∞ , whereas in the q -metric this quantity was restricted to $M_2/M_0^3 > -1/3$.

We recall that there are two photon circles for $0.13 \lesssim M_2/M_0^3 \lesssim 1.52$, whereas for lower values of the quadrupole moment, there is only one, and for higher values, there is none. The marginally stable orbit at r_{ms}^+ exists from $q = -\infty$ (corresponding to $M_2/M_0^3 = -\infty$) onwards, whereas the second marginally stable orbit at r_{ms}^- comes into existence at $q \approx 2.25$ corresponding to $M_2/M_0^3 \approx 1.52$, i.e., at the point, where the two photon circles merge and vanish. The two marginally stable orbits merge at $q \approx 5.79$, or $M_2/M_0^3 \approx 25.88$. Beyond this, any timelike circular geodesic is stable, but note that such geodesics do not exist for all radius values down to $r = 2M$. A marginally bound orbit exists from $q = -\infty$ (corresponding to $M_2/M_0^3 = -\infty$) up to $q \approx 3.91$ (or $M_2/M_0^3 \approx 7.99$).

Based on these observations we find that there are three classes of Erez-Rosen spacetimes, in close analogy to the three classes of the family of q -metrics, but expanded by a further subdivision of Class II.

Class I : $-\infty < q < 1$, i.e. $-\infty < M_2/M_0^3 \lesssim 0.13$

In class I, there is one unstable photon circle at radius r_c^+ and one marginally stable orbit at r_{ms}^+ . Orbits between infinity and r_{ms}^+ are stable, whereas orbits between r_{ms}^+ and r_c^+ are unstable. Between r_c^+ and $2M$, there are no timelike circular geodesics. This class, which contains the Schwarzschild case with $q = 0$, is completely analogous to Class I of the q -metric case.

Class IIa : $1 < q \lesssim 2.25$, i.e., $0.13 \lesssim M_2/M_0^3 \lesssim 1.52$

In this class, we have one marginally stable orbit at radius r_{ms}^+ and two photon circles, an unstable one at radius r_c^+ and a stable one at radius r_c^- . We have stable circular timelike geodesics above r_{ms}^+ , unstable ones between r_{ms}^+ and r_c^+ , no such orbits between r_c^+ and r_c^- , and again stable ones below r_c^- ; although, they may not necessarily exist all the way down to $r = 2M$. The presence of two stable regions that are separated from each other is similar to q -metrics of Class II. However, the occurrence of a region with no timelike orbits between the two stable regions is a key difference in comparison to the q -metric.

Class IIb : $2.25 \lesssim q \lesssim 4.8$, i.e., $1.52 \lesssim M_2/M_0^3 \lesssim 25.8$

In this class, we have two marginally stable orbits at radii r_{ms}^+ and r_{ms}^- . Timelike circular geodesics are stable above r_{ms}^+ and below r_{ms}^- , as far as they exist, and unstable between these values. This situation is completely analogous to Class II of q -metrics.

Class III : $4.8 \lesssim q < \infty$, i.e., $25.8 \lesssim M_2/M_0^3 < \infty$

In class III, there are no marginally stable circular orbits. All circular timelike geodesics are stable; however, circular timelike geodesics do not exist all the way down to $r = 2M$. Again, this is analogous to Class III of q -metrics.

The specific angular momentum of the marginally stable and marginally bound orbits can be found by inserting the radius values r_{ms}^\pm and r_{mb} , respectively, into the expression for the Keplerian specific angular momentum in Eq. (62). The resulting values of l_{ms}^\pm and l_{mb} are plotted in figure 8, depending on M_2/M_0^3 .

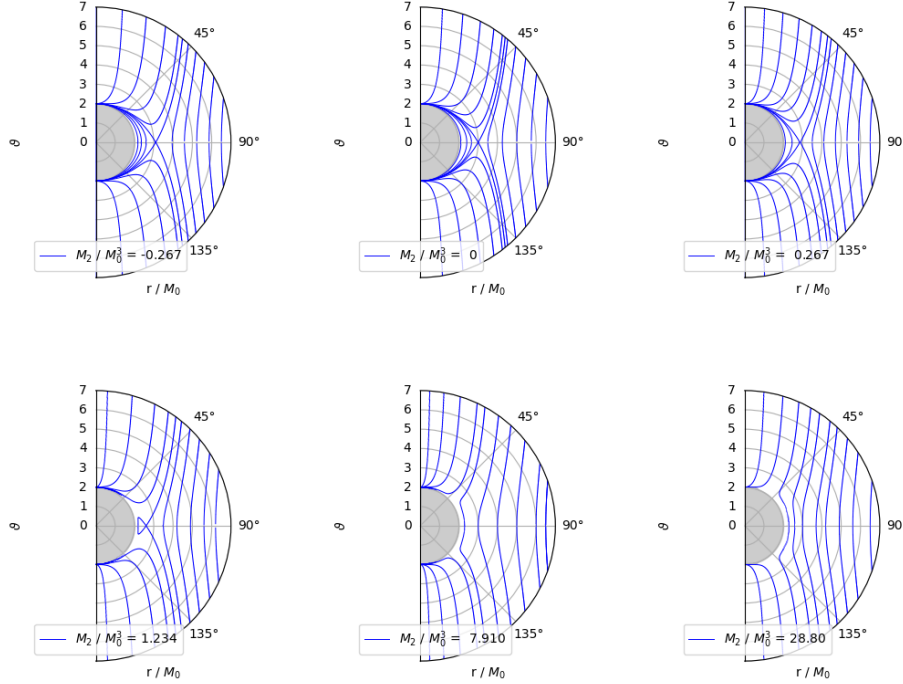


Figure 9. Von-Zeipel cylinders for different mass quadrupole moments in the Erez-Rosen spacetime. Upper row left: Class I spacetime with a negative value of M_2/M_0^3 , corresponding to an oblate geometry; upper row middle: Schwarzschild spacetime; upper row right: Class I spacetime with a positive value of M_2/M_0^3 , corresponding to a prolate geometry; lower row left: Class IIa spacetime; lower row middle: Class IIb spacetime; lower row right: Class III spacetime.

4.2. Von-Zeipel cylinders

In this section, the von-Zeipel cylinders are calculated in the Erez-Rosen spacetime. They give an insight into the behaviour of fluids in circular motion in this spacetime. Recall that the von Zeipel cylinders are defined as the surfaces $\mathcal{R} = \text{const.}$, with \mathcal{R} given by Eq. (8), and that they are independent of l (or Ω). In the Erez-Rosen spacetime, \mathcal{R} reduces to

$$\mathcal{R}(r, \vartheta)^2 = e^{4qP_2(\cos \vartheta)Q_2(r/M-1)} \frac{r^2}{\left(1 - \frac{2M}{r}\right)}. \quad (64)$$

Plots of the von Zeipel cylinders can be found in figure 9.

As in any other asymptotically flat spacetime, the von Zeipel cylinders approach flat cylinders far away from the vertical axis. At the position of an unstable photon circle, the corresponding cylinder has a self-crossing, as is the case e.g. in the Schwarzschild spacetime at $(r = 3M_0, \vartheta = \pi/2)$. For negative values of M_2/M_0^3 , the radius coordinate

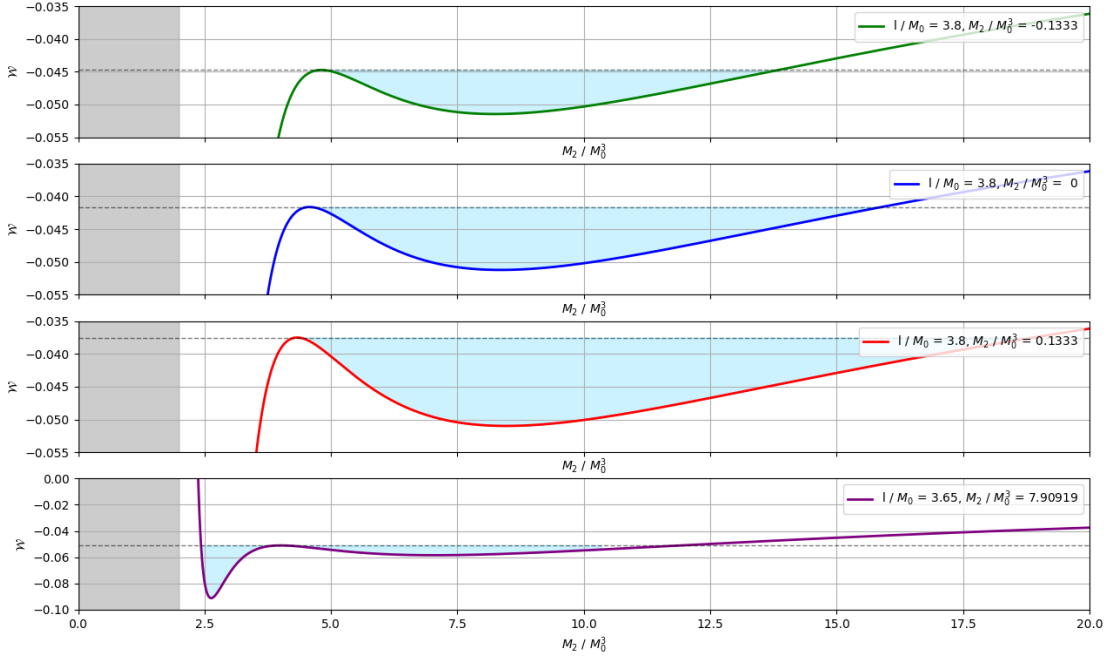


Figure 10. Effective potential in the equatorial plane in Erez-Rosen spacetime, depending on M_2/M_0^3 . The grey shaded area indicates the region bounded by the singularity at $r = 2M_0$, the lighter blue-shaded area is the region occupied by a torus filling its Roche lobe completely. Upper graph: Class I spacetime with a negative value of M_2/M_0^3 , corresponding to an oblate geometry; upper-middle graph: Schwarzschild spacetime; lower-middle graph: Class I spacetime with a positive value of M_2/M_0^3 , corresponding to a prolate geometry; lower graph: Class IIb spacetime, note that effective potential approaches $+\infty$ for $r \rightarrow r_{\text{sing}}$.

of the unstable photon circle is bigger than $3M_0$; for positive values of M_2/M_0^3 , it is smaller. Beyond $M_2/M_0^3 \approx 1.56$, where there is no photon circle anymore, no von Zeipel cylinder has a self-crossing.

Note that, in Erez-Rosen spacetimes of Class IIa, there are von Zeipel “cylinders” that actually have the topology of a torus. Such “von Zeipel tori” occur near a stable circular light ray, see the picture on the left in the lower row of figure 9. They have been observed even in spherically symmetric and static spacetimes before, e.g. in interior Schwarzschild solutions, see Abramowicz et al. [23].

4.3. Effective potential

To construct Polish doughnuts in the Erez-Rosen spacetime, we calculate the effective potential (see Eq. (12)):

$$\mathcal{W} = \frac{1}{2} \ln \left[\frac{r^2(r - 2M) \sin^2 \vartheta e^{-2qP_2(\cos \vartheta)Q_2(r/M-1)}}{r^3 \sin^2 \vartheta - l^2(r - 2M) e^{-4qP_2(\cos \vartheta)Q_2(r/M-1)}} \right]. \quad (65)$$

As before in the q -metric, we plot this potential in the equatorial plane for four different pairs of values $(l/M_0, M_2/M_0^3)$ in figure 10, and we plot correspondingly constructed Polish doughnuts in figures 11 and 12. We note that, again, the effective potential satisfies condition (15) and that, for any values of q and l , it approaches 0 from below for $r \rightarrow \infty$.

For spacetimes of Class I, we have, in complete analogy to the q -metric case, one marginally stable orbit at radius r_{ms}^+ , a marginally bound orbit at radius r_{mb} and one unstable photon orbit at radius r_c^+ , where $2M < r_c^+ < r_{\text{mb}} < r_{\text{ms}}$. The potential $\mathcal{W}(l, r, \pi/2)$ approaches $-\infty$ for $r \rightarrow 2M$. For $l^2 > l_{\text{ms}}^+$, it has a minimum at r_{cen} , and maximum at r_{cusp} . Therefore, by choosing $l^2 > l_{\text{ms}}^+$, we can construct the same type of doughnuts as for Class I in the q -metric case, see the first three panels in figure 10 and figure 11. In all cases, we have chosen $l^2 < l_{\text{mb}}$, guaranteeing that the Roche lobe features a cusp, and we have chosen \mathcal{W}_{in} in such a way that the fluid fills its Roche lobe completely. In this way we get Polish doughnuts that are quite similar to the tori in the Schwarzschild spacetime. Of course, the shape of the Roche lobe is influenced by the quadrupole moment, but qualitatively there is no difference to the Schwarzschild case.

In spacetimes of Class II, the doughnuts are similar to those in the q -metric case of the corresponding class. Recall that here Class II is subdivided into Class IIa and Class IIb. In Class IIa, there is one marginally stable orbit at radius r_{ms}^+ , a marginally bound orbit at radius r_{mb} and two photon circles at radii r_c^\pm , where $2M < r_c^- < r_c^+ < r_{\text{mb}} < r_{\text{ms}}^+ < \infty$; in the Class IIb, there is one marginally stable orbit at radius r_{ms}^+ , possibly a marginally bound orbit at radius r_{mb} , and another marginally stable orbit at radius r_{ms}^- , where $2M < r_{\text{ms}}^- (< r_{\text{mb}}) < r_{\text{ms}}^+ < \infty$. In either case, there are two separated stable regions, and this is the reason why Polish doughnuts in Class IIa spacetimes are qualitatively similar to the ones in Class IIb spacetimes. By choosing $l^2 > (l_{\text{ms}}^+)^2$, we can construct the same kind of double torus as in the q -metric case, see the lower panel of figure 10 and figure 12. As the latter figure demonstrates, the cross-section of the Roche lobes of such double tori indicate the same fish-like shape as in the q -metric case. Again, we emphasise that the “fish-tail” is isolated from the singularity at $r = 2M$. As long as the marginally bound orbit exists, we have to choose $l^2 < l_{\text{mb}}$ if we want to have two finite Roche lobes that meet in touching cusps. If the marginally bound orbit does not exist anymore, any value $l^2 > l_{\text{ms}}^+$ will do. As in the case of the q -metric, we can choose \mathcal{W}_{in} so big that the double torus becomes a single torus with two centres, see the picture on the left in figure 12.

Finally, in Erez-Rosen spacetimes of Class III, all timelike circular geodesics are stable. Therefore, we have exactly the same type of Polish doughnuts without a cusp as in the corresponding q -metric case.

Note that, again, we have assumed that the spacetime geometry is given by the unperturbed Erez-Rosen metric, neglecting the self-gravity of the torus. This is justified only as long as the density of the fluid is small enough. For the examples shown in figure 11 and 12, we demonstrate that indeed at the centre of the torus the density squared is much smaller than the Kretschmann scalar.

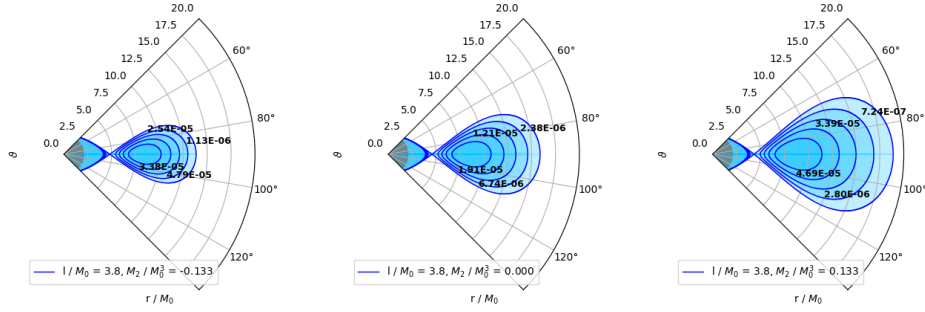


Figure 11. Polar dependency of the effective potential in the Erez-Rosen metric; black numbers represent the density in units of M^{-2} where we assumed, again, a polytropic equation of state with $K = 0.2$ and $\Gamma = 5/3$. For each torus we compare the density ρ with the Kretschmann scalar \mathcal{K} at the centre to demonstrate that the self-gravity of the fluid is negligible. Left: Class I spacetime with a positive value of M_2/M_0^3 , corresponding to a prolate geometry, $\rho(r_{\text{cen}})^2/\mathcal{K}(r_{\text{cen}}) = 5,45 \times 10^{-5}$; middle: Schwarzschild spacetime, $\rho(r_{\text{cen}})^2/\mathcal{K}(r_{\text{cen}}) = 1.18 \times 10^{-6}$; right: Class I spacetime with a negative values of M_2/M_0^3 , corresponding to an oblate geometry, $\rho(r_{\text{cen}})^2/\mathcal{K}(r_{\text{cen}}) = 2.39 \times 10^{-5}$.

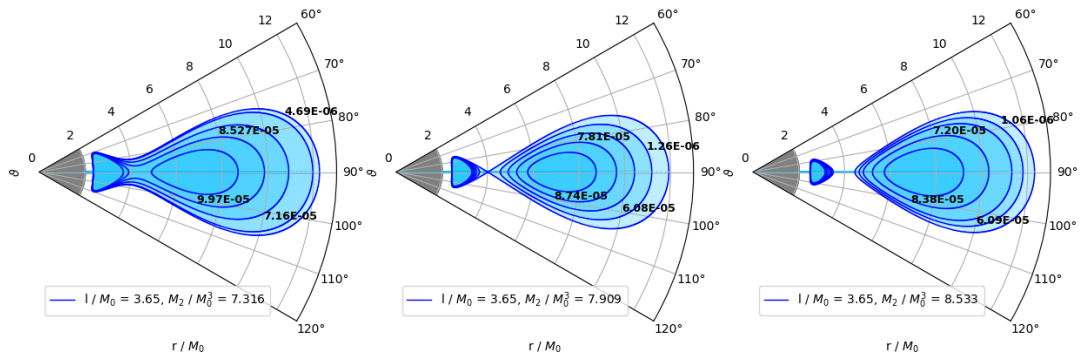


Figure 12. Polar dependency of the effective potential in an Erez-Rosen metric of Class II, for connected double tori (left panel), touching double tori (middle panel) and spatially separated tori (right panel). The black numbers represent the density in units of M_0^{-2} where we assumed again a polytropic equation of state with $K = 0.2$ and $\Gamma = 5/3$: left: $\rho(r_{\text{cen}})^2/\mathcal{K}(r_{\text{cen}}) = 2.66 \times 10^{-5}$; middle: $\rho(r_{\text{cen}})^2/\mathcal{K}(r_{\text{cen}}) = 2.33 \times 10^{-5}$; right: $\rho(r_{\text{cen}})^2/\mathcal{K}(r_{\text{cen}}) = 2.04 \times 10^{-5}$.

5. Conclusions

In this paper, we discussed geometrically thick accretion tori in two quadrupolar spacetimes, the q -metric and the Erez-Rosen spacetime. It was our main goal to find out if there are new qualitative features that distinguish these tori from analogously constructed ones in the Schwarzschild spacetime. We have seen that, both in the q -metric and in the Erez-Rosen spacetime, there are three classes to be distinguished, depending on the value of the Geroch-Hansen quadrupole moment M_2 (choosing the ADM mass M_0 as the unit of length). Class I comprises all spacetimes with (allowed) negative values of M_2 and also those with positive M_2 up to a certain value $M_2^{(1)}$. The tori in this class are similar to the tori in the Schwarzschild spacetime, which is contained as a special case in Class I. While the precise shape of a torus and the position of its outer and inner edges do depend on the quadrupole moment, there is no influence on the qualitative features. Then there is a Class III which comprises all spacetimes with positive quadrupole moment bigger than a certain value $M_2^{(2)}$. The major difference compared to Class I is in the fact that the tori *cannot* have a cusp, i.e., they cannot be at the verge of accretion, whereas in Class I the torus has a cusp if the parameters are chosen appropriately. Interesting new features arise in Class II, i.e., in spacetimes with a positive quadrupole moment between $M_2^{(1)}$ and $M_2^{(2)}$. There it is possible to construct *double tori*, both of finite size and bounded away from the naked singularity and from infinity. The meridional cross-section of such a double torus has the shape of a fish if the two Roche lobes are filled completely, with the outer torus corresponding to the body of the fish and the inner one to the fish-tail. As the inner Roche lobe has a cusp on its outer side and the outer Roche lobe has a cusp on its inner side, the fluid does not “spill over” if it extends beyond the Roche lobes; rather, it forms a single torus with two centres. These double tori, and also the single tori with two centres, are new features which do not occur in the Schwarzschild spacetime. However, perfect-fluid configurations in the form of double tori have also been found in the Kerr spacetime, for certain values of the parameters, by Pugliese et al. [16, 17]. Moreover, it is known that *charged* fluid configurations can form such double tori on the Schwarzschild spacetime in the presence of a magnetic field, see Trova et al. [18]. In particular in the latter case, the double tori are similarly shaped as the ones we have found here. So, if we ever observe such double tori we will have to investigate if there are any indications for a significant net charge of the fluid and for the presence of a magnetic field. If there are no such indications, then it would be justified to conjecture that the central object is a black hole impostor with a non-zero quadrupole moment.

Acknowledgements

We wish to thank Dennis Philipp for an important comment. Moreover, we gratefully acknowledge support from Deutsche Forschungsgemeinschaft within the Research Training Group 1620 “Models of Gravity”.

References

- [1] Abbott B P et al (LIGO Scientific Collaboration and Virgo Collaboration) 2016 Observation of gravitational waves from a binary black hole merger *Phys. Rev. Lett.* **116** 6
- [2] Jaroszynski M, Abramowicz M A and Paczynski B 1980 Supercritical accretion disks around black holes *Acta Astron.* **30** 1 1
- [3] Rezzolla L and Zanotti O 2015 *Relativistic Hydrodynamics* (Oxford: Oxford University Press)
- [4] Quevedo H 2011 Mass quadrupole as a source of naked singularities *Int. J. Mod. Phys. D* **20** 1779
- [5] Erez G and Rosen N 1959 The gravitational field of a particle possessing a multipole moment *Bull. Research Council Israel* **F.8** 47
- [6] Abramowicz M A 1971 The relativistic von Zeipel's theorem *Acta Astron.* **21** 81
- [7] Quevedo H, Toktarbay S and Yerlan A 2013 Quadrupolar gravitational fields described by the q -metric *Int. J. Math. Phys.* **3** 133
- [8] Bach R 1992 Neue Lösungen der Einsteinschen Gravitationsgleichungen *B Math. Z.* **13** 119
- [9] Zipoy D M 1966 Light fluctuation due to an intergalactic flux *Phys. Rev.* **42** 825
- [10] Voorhees B H 1970 Static axially symmetric gravitational fields *Phys. Rev. D* **2** 2119
- [11] Toktarbay S and Quevedo H 2014 A stationary q -metric *Gravit. Cosmol.* **20** 252
- [12] Stewart B W, Papadopoulos D, Witten L, Berezhdivin R and Herrera L 1982 An interior solution for the gamma metric *Gen. Rel. Grav.* **14** 97
- [13] Frutos-Alfaro F and Soffel M 2018 On relativistic multipole moments of stationary space-times *Roy. Soc. Open Sci.* **5** 180640
- [14] Frutos-Alfaro F, Quevedo H and Sanchez P 2018 Comparison of vacuum static quadrupolar metrics *Roy. Soc. Open Sci.* **5** 170826
- [15] Boshkayev K, Gasperín E, Gutiérrez-Piñeres A C, Quevedo H and Toktarbay S 2016 Motion of test particles in the field of a naked singularity *Phys. Rev. D* **93** 2
- [16] Pugliese D and Montani G 2015 Relativistic thick accretion disks: Morphology and evolutionary parameters *Phys. Rev. D* **91** 083011
- [17] Pugliese D and Stuchlík Z 2017 Ringed accretion disks: Evolution of double toroidal configurations *Astrophys. J. Suppl. Ser.* **229** 40
- [18] Trova A, Hackmann E, Karas V, Schroven K, Kovář J and Slaný P 2020 Influence of test charge and uniform magnetic field on charged fluid equilibrium structures *Phys. Rev. D* **101** 8
- [19] Young J H and Coulter C A 1969 Exact metric for a nonrotating mass with a quadrupole moment *Phys. Rev.* **184** 1313
- [20] Quevedo H and Parkes L 1989 Geodesics in Erez-Rosen space-time *Gen. Rel. Grav.* **21** 10 1047
- [21] Castejon-Amenedo J and Manko V S 1990 Superposition of the Kerr metric with the generalized Erez-Rosen solution *Phys. Rev. D* **41** 2018
- [22] Quevedo H 1990 Multipole moments in general relativity —Static and stationary vacuum solutions *Fortschr. Phys.* **38** 733
- [23] Abramowicz M A, Miller J C and Stuchlík Z 1993 Concept of radius of gyration in general relativity *Phys. Rev. D* **47** 1440